Discrete Dislocation Plasticity

van der Giessen, Erik; Needleman, A.

Published in:
Handbook of Materials Modeling

3.4

DISCRETE DISLOCATION PLASTICITY

E. Van der Giessen[1] and A. Needleman[2]
[1] *University of Groningen, Groningen, The Netherlands*
[2] *Brown University, Providence, RI, USA*

Plastic deformation of crystalline solids is of both scientific and technological interest. Over a wide temperature range, the principal mechanism of plastic deformation in crystalline solids involves the glide of large numbers of dislocations. As a consequence, since the 1930s, when dislocations were identified as carriers of plastic deformation in crystalline solids, there has been considerable interest in elucidating the physics of individual dislocations and of dislocation structures. Major effort has also been devoted to developing tools to solve boundary value problems based on phenomenological continuum descriptions in order to predict the plastic deformations that result in structures and components from some imposed loading. Since the 1980s these two approaches have grown toward each other, driven by, for instance, miniaturization and the need for more accurate models in engineering design. The approaches meet at a scale where the collective behavior of individual dislocations controls phenomena. This encounter, together with continuously increasing computing power, has fostered the development of an approach where boundary value problems are solved with plastic flow modeled in terms of the collective motion of discrete dislocations represented as line defects in a linear elastic continuum [1, 2]. This is the field of discrete dislocation plasticity.

A dislocation is a line defect in a crystalline solid which bounds the region on a plane where the material above and below are shifted relative to each other. This shift is termed the slip and the key geometric ingredient of discrete dislocation plasticity is the Burgers vector that characterizes the magnitude and direction of the slip. As a consequence of slip the displacement field is not continuous. The associated stress, strain and rotation fields are continuous except on the dislocation line where they are singular. The state near the dislocation line, the dislocation core region, is not accurately represented by linear elasticity theory. However, atomistic simulations have shown that the linear

S. Yip (ed.),
Handbook of Materials Modeling, 1115–1131.

elastic fields give an excellent description of the displacement fields beyond 8–10 Burgers vectors from the core, so that also stress and deformation are described well by the linear fields.

A discrete dislocation model of plastic flow entails the simulation of the evolution of the dislocation structure in response to a prescribed loading. The history dependence of plastic deformation is thus contained in the history of the dislocation structure. The physical mechanisms that underlie phenomena such as dislocation glide, annihilation, cross slip, etc. are governed by core-level atomic-scale events and their governing properties are supplied in the form of constitutive rules. In this section, we outline discrete dislocation plasticity, giving a perspective on key assumptions, capabilities and limitations.

1. Discrete Dislocation Dynamics

The aim is to determine the quasi-static evolution of the deformation and stress states for a dislocated solid subject to some prescribed loading history. This is done in an incremental manner in time. At a given instant, the stress state and dislocation structure are presumed known. An increment of loading is prescribed, and (i) the updated deformation and stress state, and (ii) the change in the dislocation structure need to be computed. The dislocations are represented as line singularities in a linear elastic solid. The long range interaction between dislocations is determined directly from elasticity theory, but constitutive rules are required for dislocation motion, dislocation nucleation, dislocation annihilation and, possibly, other short range interactions.

Each time step involves three main computational stages: (i) determining the driving force for dislocation motion; (ii) determining the rate of change of the dislocation structure, which involves the motion of dislocations, the generation of new dislocations, their mutual annihilation, and their possible pinning at obstacles; and (iii) determining the stress and strain state for the updated dislocation arrangement.

The key idea for determining the stress and deformation state of the solid given the current dislocation structure is superposition. The equilibrium stress and strain fields associated with the individual dislocations are singular, but they are known analytically [1, 2]. For a body with specified boundary conditions, the actual stress and deformation fields can be written as the sum of the singular fields associated with the individual dislocations and a non-singular image field that enforces the boundary conditions. The advantage of this superposition is that while standard numerical methods for elasticity problems such as finite element, finite difference or boundary element methods cannot accurately represent the strongly singular individual dislocation fields, they can accurately resolve the image fields.

The governing equations to be satisfied at time t are:

- Equilibrium,

$$\frac{\partial \sigma_{ij}}{\partial x_j} = 0, \tag{1}$$

together with $\sigma_{ij} = \sigma_{ji}$.
- The constitutive relation,

$$\sigma_{ij} = L_{ijkl}\epsilon_{kl}, \tag{2}$$

where L_{ijkl} are the components of the tensor of elastic moduli.
- The strain-displacement relation,

$$\epsilon_{ij} = \frac{1}{2}\left(\frac{\partial u_i}{\partial x_j} + \frac{\partial u_j}{\partial x_i}\right). \tag{3}$$

For a dislocated solid, the strain field does *not* satisfy compatibility, i.e.,

$$\oint_C u_{i,j}\, \mathrm{d}s \neq 0 \tag{4}$$

since the displacement field is not a continuous single-valued function.
- Boundary conditions, i.e., either prescribed displacements U_i^0 or prescribed tractions $\sigma_{ij}n_j = T_i^0$ on the boundary with outward unit normal n_i.

The total displacement, u_i, strain, ϵ_{ij}, and stress, σ_{ij} fields are written as

$$u_i = \tilde{u}_i + \hat{u}_i\,, \quad \epsilon_{ij} = \tilde{\epsilon}_{ij} + \hat{\epsilon}_{ij}\,, \quad \sigma_{ij} = \tilde{\sigma}_{ij} + \hat{\sigma}_{ij} \text{ in } V, \tag{5}$$

respectively. The $\tilde{(\ )}$ fields are the superposition of the fields of the individual dislocations, in their current configuration, i.e.,

$$\tilde{u}_i = \sum_I u_i^I\,, \quad \tilde{\epsilon}_{ij} = \sum_I \epsilon_{ij}^I\,, \quad \tilde{\sigma}_{ij} = \sum_I \sigma_{ij}^I \quad (I = 1, \ldots, N) \tag{6}$$

where $(\ )^I$ denotes the singular field associated with an individual dislocation, N being the number of dislocations in the current configuration. The $\tilde{(\ )}$ fields give rise to tractions $\tilde{T}_i$ and displacements $\tilde{U}_i$ on the boundary of the body.

The $\hat{(\ )}$ fields represent the image fields that correct for the actual boundary conditions on S. The governing equations for the $\hat{(\ )}$ fields are

$$\frac{\partial \hat{\sigma}_{ij}}{\partial x_j} = 0\,, \quad \hat{\epsilon}_{ij} = \frac{1}{2}\left(\frac{\partial \hat{u}_i}{\partial x_j} + \frac{\partial \hat{u}_j}{\partial x_i}\right) \tag{7}$$

$$\hat{\sigma}_{ij} = L_{ijkl}\hat{\epsilon}_{kl} \tag{8}$$

$$\begin{aligned} \hat{\sigma}_{ij} n_j &= \hat{T}_i = T_i^0 - \tilde{T}_i \quad \text{on } S_T \\ u_i &= \hat{U}_i = U_i^0 - \tilde{U}_i \quad \text{on } S_u \end{aligned} \tag{9}$$

Here, S_T is the portion of the boundary on which tractions are prescribed and S_u is the portion of the boundary on which displacements are prescribed, as illustrated in Fig. 1. A key point is that the $\hat{(\ )}$ fields are smooth, so that Eqs. (7)–(9) constitute a conventional linear elastic boundary value problem that can be conveniently solved by a conventional numerical method for linear elasticity problems. To date, only the finite element method has been used for this purpose, but other methods are also suitable and, for example, boundary element methods may have advantages for three-dimensional problems.

The driving force for dislocation evolution is the Peach–Koehler force which is the configurational force associated with a change in dislocation position. With Π denoting the potential energy, the Peach–Koehler force $\mathbf{f}^I$ on dislocation I is given by

$$\delta\Pi = -\sum_I \int_{\mathcal{L}^I} \mathbf{f}^I \cdot \delta\mathbf{s}^I \, \mathrm{d}l \tag{10}$$

where $\mathcal{L}^I$ denotes dislocation line I and $\delta\mathbf{s}^I$ is the change in its position.

With $\mathbf{t}^I$ a unit vector tangent to dislocation line I and $\mathbf{m}^I$ a unit vector normal to its glide plane, the local glide direction is $\mathbf{t}^I \times \mathbf{m}^I$ and the component of the Peach–Koehler force in the glide direction, f^I, is

$$f^I = m_i^I \left(\hat{\sigma}_{ij} + \sum_{J \neq I} \sigma_{ij}^J \right) b_j^I \tag{11}$$

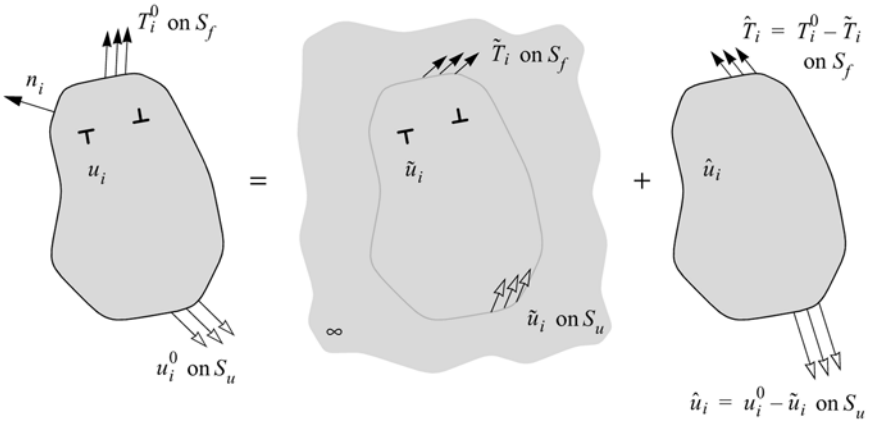

Figure 1. Decomposition into the problem of interacting dislocations in an infinite solid, the $\tilde{(\ )}$ fields, and the complementary problem for the finite body without dislocations, the $\hat{(\ )}$ or image fields.

Here, b_j^I are the components of the Burgers vector of dislocation I. Note that the value of f^I does not depend on any specification of core properties. This is because the Peach–Koehler force is calculated for a translation of the dislocation. An actual dislocation motion will, in general, involve a change in dislocation shape and thus a change in dislocation line length. The change in line length is accounted for through a constitutive rule and is referred to as the line tension. Dislocations can change glide planes (cross slip) and climb (motion off a glide plane), particularly at temperatures that are a significant fraction of the melting temperature, but attention here is confined to glide.

Any effect of geometry changes is neglected in the formulation described above. Large deformations occur inside dislocation cores and these are not modeled by the linear elastic description of dislocations. However, outside dislocation cores, finite-deformation effects can come into play once significant slip has occurred. In particular, there are effects of lattice reorientation on dislocation glide and of geometry changes on the momentum balance. It is known from continuum slip crystal plasticity that lattice reorientation effects can have a significant on the overall response. Effects of geometry changes arise in two contexts: (i) overall shape change, as in the reduction of cross-sectional area in a plastically deformed tensile bar and (ii) the formation of surface slip steps and the resulting stress concentration that occurs there. Effects of overall shape changes also occur in continuum plasticity, but the possible formation of slip steps is an additional feature of discrete dislocation plasticity. A finite deformation discrete dislocation plasticity framework has been presented by Deshpande *et al*. [3]. Here, we will confine attention to the formulation with geometry changes neglected.

2. Three-Dimensional Dislocation Dynamics

The geometry of a dislocation is governed by a number of variables:

- the slip plane, denoted with its unit normal vector $\mathbf{m}$;
- the dislocation line as a parameterized line on this plane and with a local tangent vector $\mathbf{t}$;
- the Burgers vector $\mathbf{b}$.

There are a few special parts of a generic loop, namely

$$\text{edge:} \quad \mathbf{b} \cdot \mathbf{t} = 0\,; \tag{12}$$

$$\text{screw:} \quad \mathbf{b} \cdot \mathbf{t} = \pm b\,, \tag{13}$$

b being the length of $\mathbf{b}$: $b = |\mathbf{b}|$. Edge and screw dislocations are the central notions in two-dimensional studies, as discussed in a subsequent section.

The first step in discrete dislocation plasticity in three dimensions is the description of the individual dislocations. Most methods currently in use, involve discretization of each dislocation. These schemes vary from a screw–edge representation (e.g., [4]), a representation with straight segments, e.g., [5–7], to one with a spline representation [8]. The representation of dislocation loops by straight segments, as illustrated in Fig. 2, implies that each segment has in general a mixed nature, $0 \leq |\mathbf{b} \cdot \mathbf{t}| \leq b$. The advantage of this discretization within the superposition framework is that the fields of straight segments are known exactly for a linear elastic isotropic medium. The expressions for the stress fields of individual segments in infinite space are given by Hirth and Lothe [1] while the corresponding displacement fields can be found in [9].

The topology of the discretized loop illustrated in Fig. 2 is at any instant characterized by the set $\mathbf{x}_A$ of positions of the nodes $A = 1, \ldots, N$. Assuming glide motion only, the velocity of any node, $\mathbf{v}_A$, can be written as $\mathbf{v}_A = v_A \mathbf{t} \times \mathbf{m} = v_A \mathbf{s}$. The velocity at any point $\mathbf{x}(l)$ is obtained by linear interpolation between the nodal velocities v_A. Assuming over-damped motion along the entire dislocation loop, the velocity $v(l)$ can be related to the local Peach–Koehler force $\mathbf{F}(l)$ projected onto $\mathbf{s}$ via the drag relationship

$$F(l) = Dv(l)$$

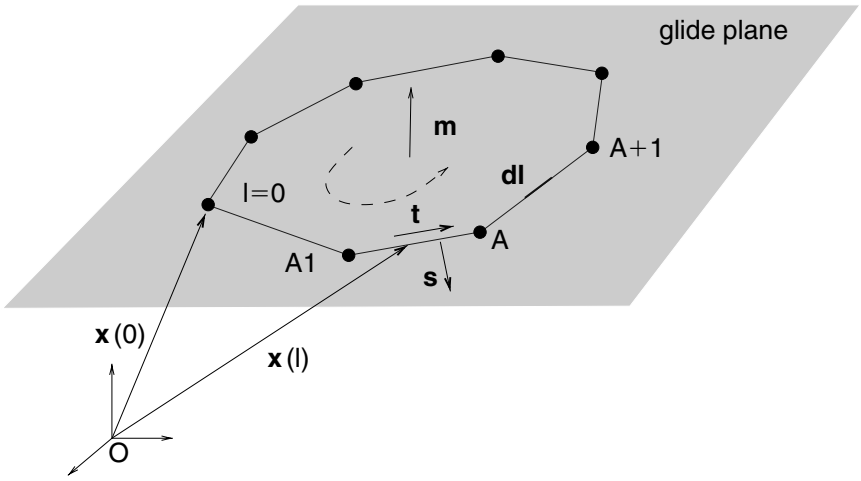

Figure 2. Description of a dislocation loop in its glide plane; **m** is the normal to the glide plane; the orientation of the loop is determined by the local tangent vector **t** and the Burgers **b**; **s** is defined as $\mathbf{t} \times \mathbf{m}$. A loop is confined to its glide plane.

with $F = \mathbf{F} \cdot \mathbf{s}$. Treating the discretized dislocation loop through a one-dimensional finite element discretization, the dynamics of the loop can be formulated through the set of equations [6]

$$F_A = \sum_{B=1}^{N} K_{AB} v_B \quad (A = 1, \ldots, N)$$

with K_{AB} a "stiffness" matrix that is determined by the loop geometry and the chosen shape functions, and is linear in the drag coefficient D. When the nodal Peach–Koehler forces F_A are calculated, the nodal velocities are obtained by solving this set of equations. The formulation can be extended to handle sliding nodes to treat dislocation junctions and dislocation segments leaving the crystal via a free surface.

The computation of the nodal Peach–Koehler force F_A requires care when it comes to the self-interaction, i.e., the contribution of the segments belonging to the same dislocation. In order to eliminate the singular contributions from the ends of the two adjacent segments, Brown's scheme can be used, see [6, 7]. Nevertheless, high-order Gaussian integration is generally needed to obtain convergence with a loop discretization that is not excessively fine.

There are various issues that require due attention in integrating the motion of a dislocation loop in time, which have to do with the continuous change of local curvature. Weygand *et al.* [6] have suggested (i) a two-level time stepping approach that minimizes the N^2 problem of interaction calculations and (ii) an adaptive re-discretization scheme of the dislocation. But there probably is much room to improve these numerical procedures in order to reduce the number of calculations while retaining accuracy. In particular, multipole methods [10, 11] can considerably reduce the computational time for evaluating dislocation interactions.

Experience with the superposition approach to boundary-value problems in three dimensions, so far, has revealed that the numerics are more demanding than one may expect from two-dimensional applications. First of all, higher-order finite elements seem necessary; 20-node brick elements with eight-point Gaussian integration are likely to be the minimum requirement. Even then, Weygand *et al*. [6] found that at least one to two elements are needed between the dislocation and a free surface in order for the calculated image forces to converge. Moreover, sufficiently many integration points per surface element are needed to compute the nodal forces from the long-range traction fields $\tilde{T}_i$.

The evolution of the dislocation structure may lead to events where nodal points and part of the corresponding dislocation segments leave the material. These events need to be detected when dislocation nodes are moved and proper constraints must be applied to the resulting surface nodes. To facilitate this detection, the surface of the sample is approximated by a triangular mesh in [6]. When part of a dislocation glides out of the crystal, the dislocation cannot

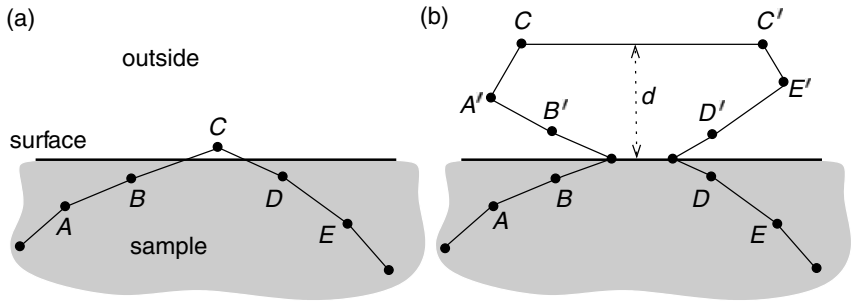

Figure 3. The pseudo-mirror construction to mimic the attractive interaction: (a) node leaves the sample; (b) surface nodes are introduced and a mirror construction is created. The view shows the projection onto the glide plane.

be treated as being open but needs has to be closed through virtual segments outside the crystal. This ensures that the analytic expressions for the stress and displacement fields remain valid and that the step produced on the surface is captured through the analytic displacement field. The error by closing the loop outside the crystal is corrected by the $(\hat{})$-solution. The shape of the virtual dislocation part is in principle irrelevant, but care needs to be taken that the strong attractive image force on the remaining dislocation from the free surface is resolved to sufficient accuracy. A judicious choice of this shape can aid the accuracy of the calculation of the dislocation – surface interaction within the finite element context. Weygand *et al.* [6] have proposed a procedure where the first two outer segments (after a surface node) are put into positions which correspond to a "mirror image" of the inner last two segments before the surface node, as shown in Fig. 3. This idea is inspired by the notion of image dislocations [1] for plane surfaces and dislocation lines parallel to that surface; for the general situation of curved dislocations on glide planes that are not orthogonal to the free surface the approach is only approximate.

3. Two-Dimensional Dislocation Dynamics

The computational complexity of discrete dislocation dynamics is substantially reduced by restricting attention to two-dimensional (2D) plane strain situations. The advantage of a 2D formulation is that complex boundary value problems can be solved with realistic dislocation densities with relatively modest computing resources. A disadvantage is that the range of phenomena that can be modeled is limited by the restricted physics of two-dimensional dislocation interactions.

Within the constraint of plane strain, the dislocations are restricted to being edge dislocations (screw dislocations are consistent with anti-plane shear deformations). For an elastically isotropic solid with shear modulus μ and Poisson's ratio ν, the stress and displacement fields at (x_1, x_2) for a dislocation with Burgers vector $b^I \boldsymbol{e}_1$ at (X_1, X_2) are:

$$\sigma_{11}^I(x_1, x_2) = -\frac{\mu b^I}{2\pi(1-\nu)} \frac{(\Delta x_2)\left[3(\Delta x_1)^2 + (\Delta x_2)^2\right]}{\left[(\Delta x_1)^2 + (\Delta x_2)^2\right]^2} \tag{14}$$

$$\sigma_{22}^I(x_1, x_2) = \frac{\mu b^I}{2\pi(1-\nu)} \frac{(\Delta x_2)\left[(\Delta x_1)^2 - (\Delta x_2)^2\right]}{\left[(\Delta x_1)^2 + (\Delta x_2)^2\right]^2} \tag{15}$$

$$\sigma_{12}^I(x_1, x_2) = -\frac{\mu b^I}{2\pi(1-\nu)} \frac{(\Delta x_1)\left[(\Delta x_1)^2 - (\Delta x_2)^2\right]}{\left[(\Delta x_1)^2 + (\Delta x_2)^2\right]^2} \tag{16}$$

$$u_1^I(x_1, x_2) = \frac{b^I}{2\pi(1-\nu)} \left[\frac{1}{2} \frac{(\Delta x_1)(\Delta x_2)}{(\Delta x_1)^2 + (\Delta x_2)^2} - (1-\nu) \tan^{-1} \frac{\Delta x_1}{\Delta x_2}\right] \tag{17}$$

$$u_2^I(x_1, x_2) = \frac{b^I}{2\pi(1-\nu)} \left[\frac{1}{2} \frac{(\Delta x_2)^2}{(\Delta x_1)^2 + (\Delta x_2)^2} - \frac{1}{4}(1-2\nu) \ln \frac{(\Delta x_1)^2 + (\Delta x_2)^2}{(b^I)^2}\right] \tag{18}$$

where $\Delta x_i = x_i - X_i$.

It can be computationally useful to take advantage of the fact that the superposition in Eq. (5) is not unique. As long as the $\tilde{(\,)}$ fields incorporate the appropriate singularities, Eqs. (14)–(18) can be extended to include any convenient non-singular fields. In particular, in circumstances where there is a traction-free surface, such as a crack surface, the gradients that the numerically computed $\hat{(\,)}$ fields need to resolve can be reduced by using the dislocation fields for a half-space. These fields are most simply expressed in terms of a complex stress function φ (the dislocation index $(\,)^I$ is omitted from φ for clarity). With the traction-free surface being the x_1-axis, with θ the angle between the Burgers vector and the x_1-axis and the dislocation position being (x_1, h), the stress and displacement fields are given by

$$\tilde{\sigma}_{22}^I - i\tilde{\sigma}_{12}^I = \varphi'(z) - \varphi'(\bar{z}) + (z - \bar{z})\overline{\varphi''(z)}, \tag{19}$$

$$\tilde{\sigma}_{11}^I + i\tilde{\sigma}_{12}^I = \varphi'(z) + \varphi'(\bar{z}) + 2\overline{\varphi'(z)} - (z - \bar{z})\overline{\varphi''(z)} \tag{20}$$

where $z = x_1 + ix_2$ and an overbar denotes the complex conjugate. The displacement components are given through

$$2\mu(\tilde{u}_1^I + i\tilde{u}_2^I) = (3 - 4\nu)\varphi(z) + \varphi(\bar{z}) - (z - \bar{z})\overline{\varphi'(z)} \tag{21}$$

with

$$\varphi(z) = \frac{\mu}{4\pi(1-\nu)}\left[i\bar{b}^I\left\{\ln\left[-m(ih-z)\right] - \ln\left[\bar{m}(ih+z)\right]\right\} + \frac{2b^I h}{z-ih}\right] \tag{22}$$

with m defined by $b^I = |b^I|m = |b^I|(\cos\theta + i\sin\theta)$.

In addition to accounting for traction-free surfaces in the ($\tilde{}$) fields, it can be convenient to use analytical fields for infinite arrays of dislocations in case of periodic boundary conditions. Expressions for walls (dislocations stacked normal to the Burgers vector) and carpets (rows of dislocations parallel to the Burgers vector) in infinite space can be found in the literature as well as for carpets of dislocations in a half space. Such solutions are characterized by being periodic in one direction and decaying exponentially in the perpendicular direction. The latter eliminates the development of artificial patterning of dislocations when using individual dislocations with their $1/r$ decay and a finite cut-off radius for dislocation-dislocation interactions.

A variety of two-dimensional analyses have been carried out so far where the magnitude of the Burgers vector is b for all dislocations and using the following set of simple constitutive rules:

- *Dislocation nucleation*: Dislocation dipoles are nucleated by simulating Frank–Read sources. In 2D this is implemented through point sources that nucleate a dislocation dipole when the Peach–Koehler force at source site I^*,

$$f^I = m_i^I\left(\hat{\sigma}_{ij} + \sum_J \sigma_{ij}^J\right)b_j = m_i^I\sigma_{ij}b_j \tag{23}$$

  equals or exceeds $b\tau_{\text{nuc}}$ during a period of time t_{nuc}, where b is the Burgers vector magnitude and τ_{nuc} and t_{nuc} are parameters specified for each source. In Eq. (23) the superscript I pertains to the source while $\sum_J \sigma_{ij}^J$ gives the stress at the source site from the individual dislocation fields. The distance L_{nuc} between the generated dislocations is taken to be given by

$$L_{\text{nuc}} = \frac{\mu}{2\pi(1-\nu)}\frac{b}{\tau_{\text{nuc}}}. \tag{24}$$

- *Dislocation glide*: The magnitude of the glide velocity v^I of dislocation I is given by

$$Bv^I = f^I - b\tau_{\text{P}} \tag{25}$$

  with B the drag coefficient and τ_{P} the Peierls stress.

*Note that the magnitude of f^I in Eq. (23) is equal to b times the local resolved shear stress.

- *Dislocation annihilation*: Annihilation of two dislocations with opposite signed Burgers vector occurs when they come within a critical annihilation distance L_e of each other.
- *Dislocation obstacles*: Obstacles to dislocation motion are modeled as fixed points on a slip plane. Pinned dislocations can only pass the obstacles when their Peach–Koehler force exceeds a specified value $b\tau_{\text{obs}}$.

Within the framework of these constitutive rules, the sources and obstacles are specified initially and do not evolve with deformation.

Two-dimensional simulations have been carried out that allow for strains of several percent and realistic dislocation densities, even in complex boundary value problems. However, the range of phenomena that can be modeled using the 2D framework is limited by the restricted physics of 2D dislocation interactions. For example, while the natural formation of dipoles at the intersection of slip planes emerges in 2D analyses, the formation of three-dimensional 3D junctions, which can be much stronger, is not accounted for. As a consequence, for example, 2D analyses of plane strain tension using the constitutive rules described above exhibit non-hardening behavior, i.e., after some initial transient plastic flow occurs at a more or less constant stress. Hardening can occur, but only when geometrically necessary dislocations are present. Recently, Benzerga *et al*. [12] have proposed dislocation constitutive rules for 2D analyses that model 3D dislocation mechanisms including dynamic junction formation, with some of the junctions serving as dislocation sources and some purely as obstacles. In this manner, the dislocation source density evolves with deformation, which is key for a realistic description of hardening. The physical background for these rules is given in [12]; here we just summarize the constitutive rules:

- *Junction formation*: The formation of a junction is taken to occur when two dislocations gliding on two intersecting slip planes approach within a specified distance d^* from the intersection point of the slip plane traces regardless of the sign of the dislocations. The intersection point is identified with the junction location and the two dislocations forming the junction are immobile until the junction is broken. When a junction forms, there is a probability p that it acts as a potential anchoring point for a Frank–Read source and a probability $(1 - p)$ that it acts as an obstacle.
- *Dynamic obstacles*: Dislocations that approach the junction are kept at a distance greater than or equal to d^* from the junction location. A junction I is destroyed if the Peach–Koehler force acting on either dislocation comprising the junction attains or exceeds the breaking force $\tau^I_{\text{brk}} b$ with

$$\tau^I_{\text{brk}} = \beta_{\text{brk}} \frac{\mu b}{\mathcal{S}^I} \tag{26}$$

Here, $\mathcal{S}^I$ is the distance to the nearest junction in any of the two intersecting planes, b is the magnitude of the Burgers vector of the dislocation

making up the junction and β_{brk} is a parameter giving the strength of the junction.

- *Source operation*: A dislocation dipole is nucleated at source I when the value of the Peach-Koehler force at the junction exceeds $\tau^I_{\text{nuc}} b$ for a time t^I_{nuc}, where

$$\tau^I_{\text{nuc}} = \beta_{\text{nuc}} \frac{\mu b}{\mathcal{S}^I} \tag{27}$$

with β_{nuc} giving the source strength and $\mathcal{S}^I$ the distance to the nearest junction on the slip plane. In evaluating $\mathcal{S}^I$ all junctions are considered regardless of whether they are anchoring points or obstacles. The time t^I_{nuc} is given by

$$t^I_{\text{nuc}} = \gamma \frac{\mathcal{S}^I}{|\tau^I| b} \tag{28}$$

where τ^I is the resolved shear stress at the junction location and γ depends on the drag coefficient B and on $\tau^I/\tau^I_{\text{nuc}}$.
For nucleation of an isolated loop,

$$L^I_{\text{nuc}} = \kappa \mathcal{S}^I \tag{29}$$

where $\kappa > 1$. However, the emitted dipole is not allowed to pass through a dislocation near the source. As a consequence, the size of the emitted loop is $\mathcal{S}^I \le L^I_{\text{nuc}} < \kappa \mathcal{S}^I$.

- *Line tension*: The energy cost associated with loop expansion is modeled through a configurational force of magnitude $\mathcal{L}^I b$ pointing from one dislocation in a dipole toward the other. The magnitude of $\mathcal{L}^I$ is

$$\mathcal{L}^I = -\alpha \frac{\mu |b|}{\mathcal{S}^I_{\text{d}}} \tag{30}$$

where α is a proportionality factor and $\mathcal{S}^I_{\text{d}}$ is the algebraic distance between the two dislocations comprising the dipole, so that the sign of $\mathcal{L}^I$ depends on the sign of $\mathcal{S}^I_{\text{d}}$. The line tension is then included in Eq. (25) by adding $\mathcal{L}^I b$ as a driving force to the right-hand side.

- *Interaction of moving dislocations with junctions*: An anchoring point can be destroyed by annihilation of one of the dislocations forming the junction. On the other hand, an obstacle can be destroyed either by annihilation or by the local stress exceeding the obstacle strength. In order to analyze the consequences of these two mechanisms, two options have been considered: (i) only junction destruction can occur when a critical stress is reached so that, as a consequence, only obstacles can be destroyed and; (ii) annihilation is possible in which case both obstacles and

anchoring points can be destroyed. In option (i), when a dislocation of opposite sign comes close to an obstacle it is pinned at a distance d^* from the obstacle, while when a dislocation of opposite sign comes close to an anchoring point the gliding dislocation is free to oscillate around the anchoring point.

Calculations using these constitutive rules also use the constitutive rules for dislocation motion, Eq. (25), and dislocation annihilation. In addition, initial static sources and obstacles can be specified. Although initial results are encouraging [12], it remains to be seen how much of 3D dislocation physics can actually be incorporated in a 2D formulation.

Computing the change in the dislocation structure in each time increment involves: (i) computing the motion of existing dislocations; (ii) checking for interactions with the static obstacles and with existing dynamic junctions; (iii) checking for dislocation annihilation; (iv) determining if any dislocations have exited at a free surface; (v) determining if any dislocations pinned at static obstacles have broken away; (vi) checking for the destruction of the dynamic junctions; (vii) checking for the creation of new dynamic junctions; (viii) checking for nucleation at the static and dynamic sources.

Since only edge dislocations are present in the 2D analyses and since nucleation involves the production of dipoles, the total Burgers vector does not change during the deformation history. The net Burgers vector in the body can only change when dislocations exit the body, leaving a step on the surface. Since edge dislocations correspond to addition or subtraction of a half-plane of atoms, conservation of total Burgers vector reflects conservation of mass.

It is worth mentioning that the constitutive relations used for dislocation nucleation pertain to nucleation from Frank–Read sources where the main issue is mainly one of propagating a loop to its stable size. Criteria for other nucleation processes, for example from surface steps or grain boundaries (which can also act as dislocation sinks), remain to be developed.

Dislocation dynamics is chaotic [13]. It seems that the chaotic behavior has relatively little effect on the predicted stress-strain response under monotonic loading, where the variations in dislocation position tend to average out, but possibly more effect on fracture predictions, where local values of stress and deformation can matter. However, the implications of this chaotic behavior remain to be fully explored.

4. Example

Experiments have shown that stress evolution in films with a thickness on the order of micrometers is size dependent. This effect cannot be resolved by classical continuum theories since they lack a material length scale. The method presented above is illustrated by considering a 2D plane strain model

of a thin film bonded to an elastic substrate, as analyzed by [14]. The film of thickness h is considered to be a single crystal and perfectly bonded to a half-infinite substrate, see Fig. 4. The single crystal contains three slip systems with slip plane orientation: $\phi^{(1)}=0^\circ$; $\phi^{(2)}=60^\circ$; $\phi^{(3)}=120^\circ$, which resembles an fcc crystal with the (110) plane coinciding with the x_1-x_2 plane of deformation.

The elastic properties of the film are assumed to be isotropic and the same as those of the substrate. Stress is caused by the mismatch in the coefficients of thermal expansion and arises from cooling from the stress-free state. This is taken into account by subtracting the thermal stress $3E\alpha\,\Delta T/(1-2\nu)$ due to a temperature difference ΔT from the left-hand side of (8), where $E=2(1+\nu)\mu$ is Young's modulus and α is the difference of the coefficient of linear thermal expansion in film, α_f, and of that in the substrate, α_s. Note that the thermal part of the problem is taken care of through the $\hat{(\,)}$ fields.

The film is infinitely long in the x_1 direction but is treated as being periodic with cell width w. The $\tilde{(\,)}$ fields are constructed from the periodic fields of a dislocation and all its replicas at mutual distance w. The traction-free condition of the film surface $x_2=h$ is accounted for by the $\hat{(\,)}$ fields. The interface between film and substrate is treated here as being impenetrable by dislocations (by putting very strong obstacles at the ends of the slip planes).

Simulations start from a stress-free and dislocation-free configuration. The film contains a random distribution of 60 sources/μm^2. The nucleation strength $\tau_{\rm nuc}$ of each source is randomly taken out of a Gaussian distribution with average $\tau_{\rm nuc}=25$ MPa and standard deviation $\tau_{\rm nuc}=5$ MPa. A dislocation dipole is generated from the source when the resolved shear stress at the source exceeds the nucleation strength for a given time $t_{\rm nuc}$ = 10 ns. There are no obstacles, and neither junction formation nor line tension is accounted for.

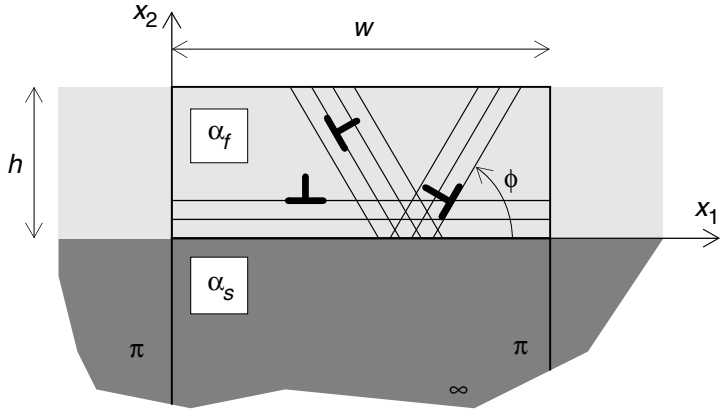

Figure 4. Geometry of the film-substrate problem. A unit cell of width w is analyzed and the height of the substrate is taken large enough to represent a half space.

Figure 5 shows how the dislocation distribution evolves from the initially dislocation- and stress-free state during cooling in a film with $h = 0.5\,\mu\text{m}$ from $T = 600\,\text{K}$. After roughly 25 K, the first dislocation dipoles are generated inside the hitherto uniform elastic stress field. One dislocation moves toward the impenetrable interface where it gets stopped, while the other exits the film at the free surface. As cooling proceeds, more and more dislocations are generated and pile up against the interface. This causes the formation of a boundary layer of relatively high stress just above the interface. The thickness of the boundary layer turns out to be more or less independent of film thickness. This gives rise to a size effect: thinner films are harder, as shown in Fig. 6. The stress-temperature curves are serrated as a consequence of the discrete nucleation events. The straight-line fits demonstrate that hardening is approximately linear with the constitutive rules adopted in this simulation. The kink in the stress-temperature curve after ∼70 K for the $h = 0.25\,\mu\text{m}$ film is caused

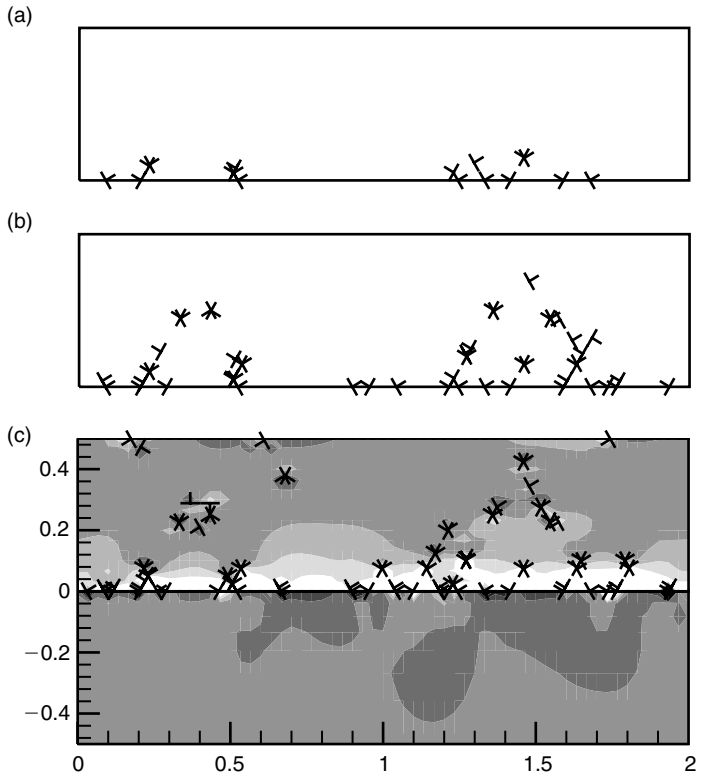

Figure 5. Evolution of the dislocation distribution inside the film during cooling by: (a) 100 K; (b) 150 K; (c) 200 K. In (c) the distribution of the stress σ_{11} parallel to the film is superimposed, also showing the top 0.5 μm of the substrate.

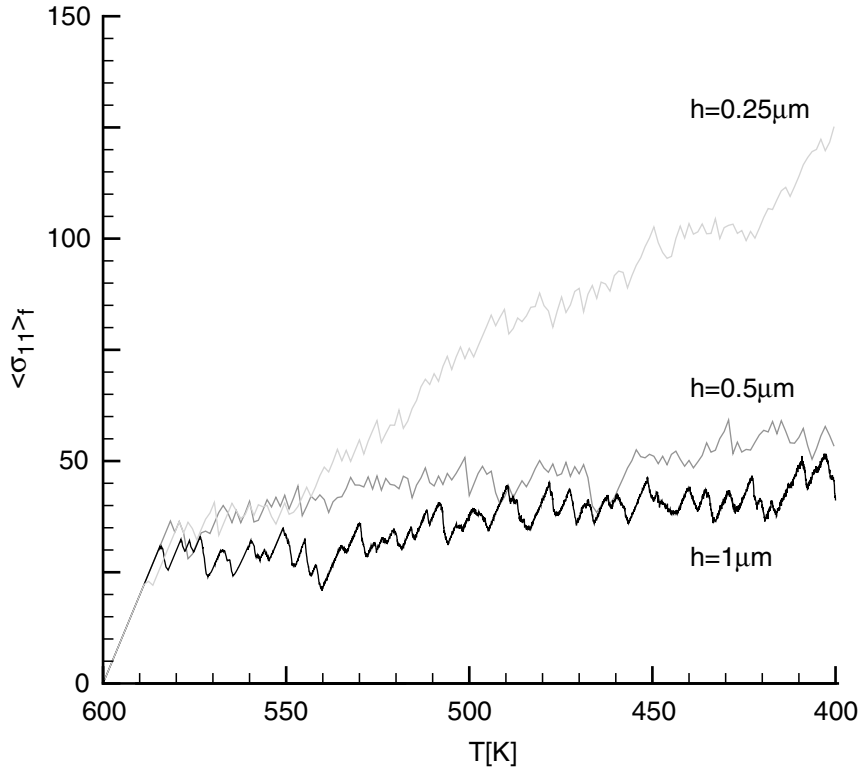

Figure 6. Average stress in the film, $\langle \sigma_{11} \rangle_f$, versus temperature for three film thicknesses.

by the limited availability of sources in such thin films [14]. Quite generally, at small size scales limited source availability can significantly affect the evolution of plastic deformation.

References

[1] J.P. Hirth and J. Lothe, *Theory of Dislocations*, 2nd edn., Wiley, New York, 1982.
[2] F.R.N. Nabarro, *Theory of Crystal Dislocations*, Oxford Univ., Press, Oxford, 1967.
[3] V.S. Deshpande, A. Needleman, and E. Van der Giessen, "Finite strain discrete dislocation plasticity," *J. Mech. Phys. Solids*, 51, 2057–2083, 2003.
[4] L.P. Kubin, G. Canova, M. Condat, B. Devincre, V. Pontikis, and Y. Bréchet, "Dislocation microstructures and plastic flow: a 3D simulation," *Solid State Phenomena*, 23-24, 455–472, 1992.
[5] H.M. Zbib, M. Rhee, and J.P. Hirth, "On plastic deformation and the dynamics of 3D dislocations," *Int. J. Mech. Sci.*, 40, 113–127, 1998.
[6] D. Weygand, L.H. Friedman, E. Van der Giessen, and A. Needleman, "Aspects of boundary-value problem solutions with three-dimensional dislocation dynamics," *Model. Simul. Mat. Sci. Engrg.*, 10, 437–468, 2002.

[7] K.W. Schwarz, "Simulation of dislocations on the mesoscopic scale. I. Methods and examples," *J. Appl. Phys.*, 85, 108–119, 1999.
[8] N.M. Ghoniem and L.Z. Sun, "Fast-sum method for the elastic field of three-dimensional dislocation ensembles," *Phys. Rev. B*, 60, 128–140, 1999.
[9] D.M. Barnett, "The displacement field of a triangular dislocation loop," *Phil. Mag. A*, 51, 383–387, 1985.
[10] G.J. Rodin, "Towards rapid evaluation of the elastic interactions among three-dimensional dislocations," *Phil. Mag. Lett.*, 77, 187–190, 1998.
[11] R. LeSar and J.M. Rickman, "Multipole expansion of dislocation interactions: application to discrete dislocations," *Phys. Rev. B*, 65, 144110, 2002.
[12] A.A. Benzerga, Y. Bréchet, A. Needleman, and E. Van der Giessen, "Incorporating three-dimensional mechanisms intodislocation dynamics," *Modelling Simul. Mater. Sci. Eng.*, 12, 159–196, 2004.
[13] V.S. Deshpande, A. Needleman, and E. Van der Giessen, "Dislocation dynamics is chaotic," *Scripta Mat.*, 45, 1047–1053, 2001.
[14] L. Nicola, E. Van der Giessen, and A. Needleman, "Discrete dislocation analysis of size effects in thin films," *J. Appl. Phys.*, 93, 5920–5928, 2003.